Predicted hcp Ag-Al metastable phase diagram, equilibrium ground states, and precipitate structure

Nikolai A. Zarkevich* and D. D. Johnson
Departments of Physics and Materials Science & Engineering, and Frederich Seitz Materials Research Laboratory, University of Illinois, Urbana-Champaign, Illinois 61801

(Received 2 September 2002; revised manuscript received 17 December 2002; published 21 February 2003)

Formation energies of a number of hcp-based Ag-Al structures are obtained from *ab initio* electronic-structure calculations and used within a cluster expansion approach to construct an effective alloy Hamiltonian. Formation energies are found to be inherently asymmetric versus composition, providing an incipient tendency for precipitation in Al-rich alloy. Both ground-state search and Monte Carlo simulations based on the cluster expansion are used to determine the metastable hcp Ag-Al phase diagram. A new equilibrium hcp AgAl ground state is predicted and zero-energy domain boundary defects are found. From thermodynamic results, we discuss the precipitate structure and composition in Al-rich Al-Ag alloys and explain recent microscopy data.

DOI: 10.1103/PhysRevB.67.064104 PACS number(s): 81.30.Bx, 61.66.Dk, 64.75.+g, 31.15.Ar

I. INTRODUCTION

Aluminum alloys are lightweight materials of continued technological importance. Precipitation strengthening in these alloys could be better understood by looking at the relevant stable and metastable phase diagrams. Due to the easy formation of both Guinier-Preston (GP) zones and hexagonal closed-packed (hcp) precipitates, the Al-Ag system continues to be studied, though its phase diagram in Fig. 1,[1,2] showing that Al-rich alloy segregates into intermediate hcp γ-phase and terminal fcc Al phase, was first established nearly a century ago.[3,4] When quenched in the metastable fcc Al-rich miscibility gap, fcc-based GP zones form, whereas, when quenched from the high-temperature terminal fcc Al-rich solid solution phase, hcp precipitates form almost instantly.[5,6]

The theoretically verified[7] ground-state structure of bulk hcp Ag_2Al was originally proposed from the measured short-range order (SRO) within the hcp basal planes,[8] which remains frozen-in below 475 K (Refs. 9 and 10) due to a negligible diffusion rate at low temperatures. Similarly, no fully long-range ordered (LRO) structure has been determined experimentally within the hcp precipitates. The present determination of the metastable hcp phase diagram was motivated by recent experimental[6] and theoretical[7] indication that the composition of hcp Ag-Al precipitates in Al-rich alloy is not Ag_2Al, but near Ag-50 at. % Al.

Here we use a cluster expansion technique based on formation energies obtained from *ab initio* electronic-structure calculations to construct the effective alloy Hamiltonian and perform ground-state search and Monte Carlo simulations. We determine the hcp ground states and compare the hcp- and fcc-based ground-state energies. We predict a yet unobserved hcp stoichiometric Ag-50 at. % Al ground state, which is 16 meV/atom lower in energy than the phase-segregated known ground states, namely, the fcc Al and ordered hcp Ag_2Al. Interestingly, we find that there is a zero-energy structural defect, which inhibits the LRO within the hcp basal planes in the new AgAl structure.

The metastable hcp Ag-Al phase diagram is constructed by performing Monte Carlo simulations; in combination with the previously published fcc diagram[11,12] shown in Fig. 2, it provides more complete information and better understanding of precipitation. In addition, we determine the hcp random solid solution mixing energies, compare them to those of the fcc-based alloy,[11] and predict the composition range for disordered hcp precipitates. We note that convex mixing energies indicate an incipient tendency for Al-rich alloys to form a miscibility gap and drive precipitation. This convexity is already observed for the measured formation enthalpy in liquid Al-Ag.[13] Finally, we discuss the predicted equilibrium hcp AgAl phase relevant to precipitation in Al-rich Al-Ag alloys and explain recent microscopy data.[6]

II. METHODS

To find the hcp Ag-Al ground states and other low-energy structures relevant to thermodynamics and to determine the metastable phase diagram, we perform Monte Carlo simulations based on a cluster-expansion (CE) Hamiltonian.[14] This

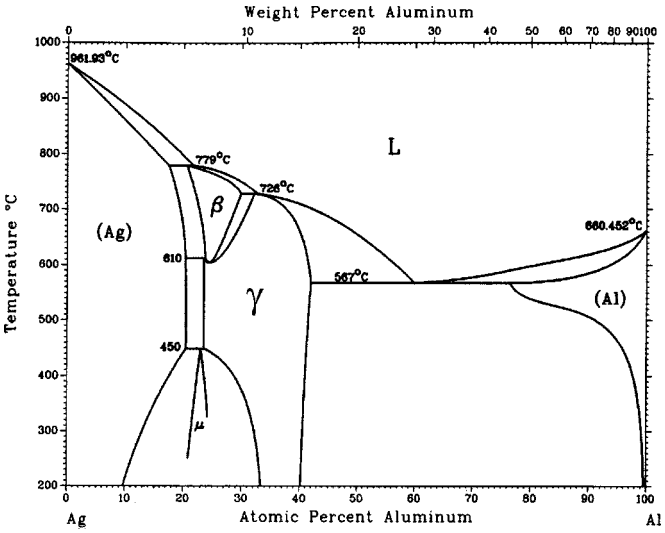

FIG. 1. The assessed Ag-Al phase diagram (Refs. 1 and 2). This figure is reprinted by permission of ASM International.

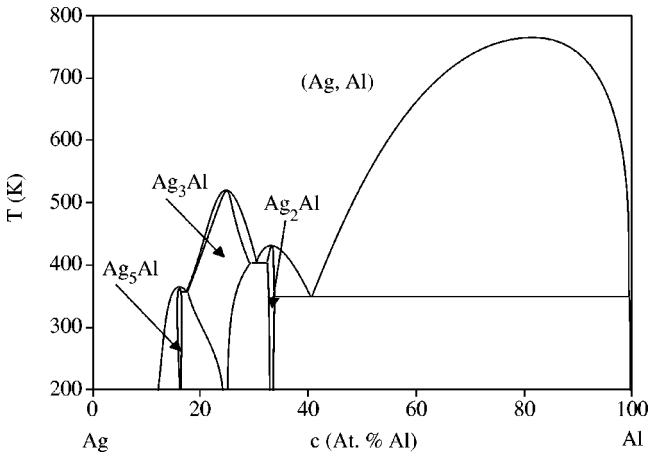

FIG. 2. First-principles calculated composition-temperature phase diagram for a metastable fcc-based Ag-Al alloy from Refs. 11 and 12.

Hamiltonian is constructed using the structural inversion method (SIM) (Refs. 14–18) from a set of structural formation energies obtained from *ab initio* electronic-structure calculations described below.

A. Electronic-structure calculations

We use the Vienna *ab initio* simulation package (VASP)[19–22] based on electronic density-functional theory (DFT) to calculate formation energies of a number of fully relaxed structures. This full-potential package with the ultrasoft pseudopotentials suggested by Vanderbilt[23] and supplied by Kresse and Hafner[24] computes atomic forces and pressure tensor to allow a full relaxation of unit cell and atomic positions within any structure. Structures are relaxed until all atomic forces are less then 30 meV/Å, and stress components do not exceed 1 kBar. We use special point method for the *k*-space Brillouin zone (BZ) integration with uniform density mesh with $N_{k-pts}\times N_{atoms}\approx 20000$ for all structures, where N_{k-pts} is the total number of *k*-points in the BZ and N_{atoms} is the number of atoms per unit cell. The cutoff energy for plane wave basis set is 200 eV. This provides convergence of calculated formation energies within ~ 1 meV/atom. See Ref. 7 for further details. The absolute accuracy of VASP energies was also addressed in Ref. 25, where the first-principles calculated and experimentally assessed formation enthalpies of some Al-rich equilibrium compounds were compared and found to be in excellent agreement.[25]

B. Structural inversion method

Any Al-Ag atomic configuration may be represented by a set of occupation variables $\{\xi_p\}$, with $\xi_p=1(0)$ if the site p is (is not) occupied by Ag. An effective alloy Hamiltonian is then constructed via a cluster expansion[14] over a truncated set of interactions:

$$H=V_0+\sum_{n,f,d} V_f^{(n)}\Phi_{fd}^{(n)}. \tag{1}$$

Here $V_f^{(n)}$ are *n*-body effective cluster interactions (ECIs), and $\Phi_{fd}^{(n)}$ are *n*-site correlation functions defined on an *n*th-order cluster of type (f,d). The sum is over all cluster types, both symmetry-distinct (n,f) and symmetry-equivalent $(d=1,\ldots,D_f^{(n)})$, and thus includes degeneracies $D_f^{(n)}$ of *n*-body clusters of symmetry-distinct types *f*. For example, for $n=2$ (two-body), $f=1$ and $d=1-6$ give six nearest neighbors within the hcp (0001) basal plane, $f=2$ $(f=3)$ gives six out-of-plane nearest (next-nearest) neighbors. The correlation functions can be written as

$$\Phi_{fd}^{(n)}=\frac{1}{N_{fd}^{(n)}}\sum_{\{p\}_{fd}^{(n)}}\xi_{p_1}\xi_{p_2}\cdots\xi_{p_n}, \tag{2}$$

where the sum is over all clusters of a given type and $N_{fd}^{(n)}$ is the total number of such clusters.

For any given ordered atomic arrangement $\sigma=\{\xi_p\}$, the energy is

$$E^{\sigma}=V_0+\sum_{n,f} V_f^{(n)}D_f^{(n)}\langle\Phi_f^{(n)}\rangle^{\sigma} \tag{3}$$

Here degeneracies $D_f^{(n)}$ and the configurational averages of the correlation functions $\langle\Phi_{fd}^{(n)}\rangle^{\sigma}$ and

$$\langle\Phi_f^{(n)}\rangle^{\sigma}=\frac{1}{D_f^{(n)}}\sum_{d=1}^{D_f^{(n)}}\langle\Phi_{fd}^{(n)}\rangle^{\sigma}$$

are just geometric constants. Given a set of ECIs, one can predict structural energies from linear equation (3). Inversely, from a chosen set of clusters and a given set of structural energies $\{E^{\sigma}\}$, one can find the ECIs by solving the system of linear equations (3).

Structural inversion can be performed either at fixed composition, yielding composition-dependent ECIs, as done in Ref. 7, or, as we do below and as is typical, over the whole composition range, producing composition-independent ECIs, see Ref. 16–18.

As we use energies of fully relaxed structures, both internal and external (sell volume and shape) static relaxations are indirectly incorporated by the SIM. If needed, large external relaxations and coherency strain within precipitates could be handled separately using elasticity theory.[17,26] Fortunately, within the Al-Ag alloys the atomic size mismatch is very small and the coherency strain is not important.[7]

C. Iterative construction of cluster expansion

We note that some structures (e.g., Ag_3Al_2 structure "n5" at $c_{Al}=0.4$) are only a few meV above the tie line connecting the ground states (see Fig. 6); they might become fictitious ground states after an inaccurate SIM fit. To avoid this problem, we iteratively construct a converged cluster expansion.

Given a set of structural energies, a CE Hamiltonian is constructed via structural inversion and used to estimate energies of a large number of atomic configurations, and to search for all ground-state candidates. Energies of predicted low-energy structures are then obtained from the first-

principles electronic-structure calculations. If the calculated *ab initio* energies differ significantly from the estimated CE ones, they are added to the set to be fitted and another iteration is performed. This iterative procedure is especially useful for systems with competing long-period structures or degenerate ground states. We note that only a converged cluster expansion, with energies of ground states and low-energy structures reproduced within a few meV, is reliable for addressing the thermodynamics.

D. Monte Carlo simulations

We use both canonical (fixed composition c) and grand canonical (both fixed chemical potential μ and fixed temperature T) Monte Carlo simulations to construct the phase diagram. The simulation box includes from $12\times12\times8$ to $24\times24\times15$ hcp unit cells with 2 atoms/cell (i.e., 2304–17280 atoms) with periodic boundary conditions imposed. The temperature step varies from 1 to 0.05 meV (at fixed μ; smaller near the transition temperature T_c). The μ step varies from 10 to 1 meV. The number of equilibration and sampling steps is 100–1000 and 4000–40 000, respectively (more near T_c and at low T). See Ref. 7 for further details.

The phase boundaries defining the T-c phase diagram are determined using Monte Carlo simulations by heating (cooling) from (dis)ordered phases at fixed c and at fixed μ, and by varying μ at fixed T starting from each intermediate ordered phase and from terminal Ag and Al solid solutions.

III. RESULTS

Below we calculated *ab initio* formation energies of 49 hcp structures (see Table I), and used them in SIM to construct a cluster expansion for hcp Ag-Al; see Table II and Fig. 3. Using the CE Hamiltonian [Eq. (1) and (2)], we performed ground-state search and Monte Carlo simulations to determine the metastable hcp Ag-Al phase diagram. We also calculated formation energies of pertinent fcc-based Ag-Al configurations (determined in Ref. 11) and estimated the hcp- and fcc-based solid solution mixing energies needed for discussion of precipitation.

A. Structures

As a starting point for our studies, we use a set of 49 hcp Ag-Al structures of various compositions. The unit cells of structures 1–32 are shown in Fig. 2 of Ref. 27. The structures (1)–(11) of stoichiometry Ag_2Al are described in Ref. 7. The hcp ground states and remaining structures (with labels in quotes) are shown in Fig. 4 and described below.

Structure 24 in Fig. 4 was suggested by Neumann[8] as the Ag_2Al ground state; structure 25 was proposed by Howe *et al.*[5] for hcp Ag_2Al precipitates; the AgAl hybrid structure "nh," based on off-stoichiometric Neumann and Howe structures, was introduced in Ref. 7. Structures "$n3$" ($AgAl_3$) and "$m3$" and "$m6$" (both Ag_5Al_3 and Ag_3Al_5) are modified from 3 and 6 by exchange of Ag and Al atoms to produce different stoichiometries. Structure "$9a$" is modified from 9. Structures "n5" and "n7" appeared as a product of the iterative procedure described in Sec. II C.

TABLE I. The DFT-calculated and SIM-fitted formation energies (in meV/atom) of fully relaxed hcp structures relative to the metastable hcp Al and Ag. The energies of the fcc-based Al and Ag are −34.0 and −6.3 meV/atom, respectively. Structures 1–32 are shown in Fig. 2 of Ref. 27; the Ag_2Al structures (1) through (11) are described in Ref. 7; the rest are described in Fig. 4 and in Sec. III A.

Structure		DFT	SIM
Ag	1	0.0	1.4
Ag_7Al	"$n7$"	−64.7	−62.4
Ag_5Al	30	−85.0	−86.5
Ag_3Al	22	−115.0	−115.7
	21	−108.9	−109.1
	23	−95.5	−102.3
Ag_2Al	24 (1)	−136.1	−135.1
	(2)	−132.6	−132.9
	27 (5)	−126.3	−125.1
	25 (6)	−117.6	−117.7
	(7)	−105.2	−116.2
	(8)	−92.0	−95.2
	28 (9)	−94.8	−93.1
	(10)	−95.5	−100.6
	(11)	−89.5	−81.0
Ag_5Al_3	"$m3$"	−131.3	−125.0
	"$m6$"	−118.4	−113.5
Ag_3Al_2	"$n5$"	−131.9	−131.3
AgAl	3	−126.5	−127.6
	6	−125.9	−124.6
	9	−109.9	−105.4
	4	−98.0	−92.6
	16	−97.5	−92.9
	20	−96.6	−92.7
	5	−96.5	−94.5
	"nh"	−96.5	−92.8
	"$3a$"	−96.3	−96.3
	14	−95.3	−96.9
	15	−93.3	−93.9
	"$9a$"	−92.3	−84.0
	13	−91.6	−100.0
	8	−91.2	−82.9
	2	−90.3	−90.3
	"$n4$"	−82.6	−82.8
	12	−76.3	−71.4
	10	−74.4	−77.4
	11	−57.3	−64.8
	"$z4$"	−56.2	−54.9
Ag_3Al_5	"$m3$"	−18.3	−27.5
	"$m6$"	−45.3	−55.6
$AgAl_2$	27	−10.1	−19.0
	25	−2.8	−4.0
	24	6.8	−0.2
$AgAl_3$	"$n3$"	16.2	22.0
	22	45.7	61.1
	21	55.8	49.6
$AgAl_5$	"$z5$"	−14.0	−16.4
$AgAl_7$	"$z7$"	−12.2	−11.9
Al	1	0.0	1.5

TABLE II. Effective cluster interactions for the clusters shown in Fig. 3. $V_0 = 1.5$ meV; $V_1 = 483.3$ meV. Numbers refer to Fig. 3 and roughly indicate the range of ECI.

	Two-body	Three-body	Four-body
1	−328.6	276.6	7.6
2	−487.0	197.5	−70.8
3	−50.2	69.8	−70.7
4	−166.9	137.2	−39.1
5	−12.6	65.1	−27.2
6	38.7	41.0	−23.3
7	14.3	−6.2	11.9
8	8.9		

The remaining AgAl structures "3a," "n4," and "z4" have the periodicity $2c$ along the c-direction. Structure "$3a$" (modified from 3) consists of two unit cells of structure 3 (or structure 2) stacked in the c direction, with all Al and Ag atoms swapped in one of the cells; its energy is expected to be between the energies of structures 2 and 3. The AgAl structure "$n4$" (modified from 24) consists of two unit cells of Ag_2Al structure 24 (see Fig. 4) stacked in the c direction, but with Al atoms only in one of the hcp (0001) planes (an Al plane). Stacking along the c-direction alternating (0001) planes of Ag and Al produces AgAl structure 4. Structure "z4" is composed of two Ag (0001) planes followed by two Al (0001) planes. Structures "z5" ($AgAl_5$) and "z7" ($AgAl_7$) are composed of five and seven Al (0001) planes, respectively, followed by one Ag (0001) plane stacked in the c direction. The unit cells of AgAl structures 3 and 6 are compared in Fig. 5, which shows a domain boundary as will be discussed in Sec. III C.

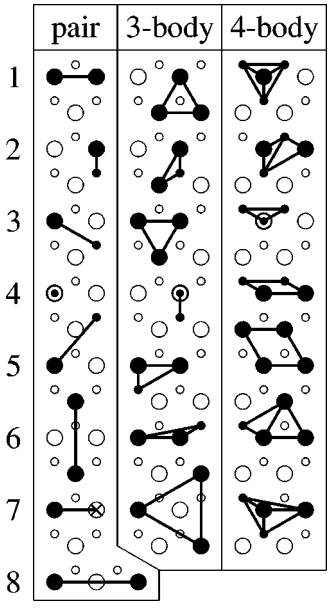

FIG. 3. The two-body (pair), three-body, and four-body clusters used in SIM in the (0001) hcp projection. Concentric circles represent two sites, one above the other, separated by a distance c. A cross represents a site in the next basal plane.

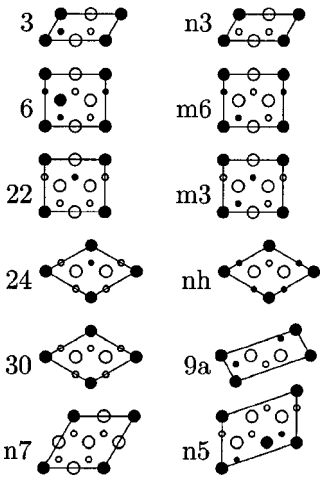

FIG. 4. The hcp ground state and other structures in hcp (0001) projection. Large (small) circles represent atoms in the A (B) planes in the hcp $ABAB$ stacking, with periodicity of $1c$ along the c-direction. For Ag-rich structures filled (empty) circles are Al (Ag) atoms. Except for the monoclinic ("$9a$"), all structures are orthorhombic (30 and "$n7$" are hexagonal).

B. Cluster Expansion for hcp Ag-Al

The *ab initio* calculated and SIM-fitted formation energies (relative to the hcp Ag and Al) of 49 fully relaxed hcp structures are listed in Table I and plotted in Fig. 6. The standard deviation for this SIM fit is $\Delta E = 4.3$ meV. The energies of low-energy structures, which are more important for thermodynamics, are reproduced significantly better (the ground-state energies are within 1.5 meV).

We have used 24 ECIs listed in Table II (clusters are shown in Fig. 3), including constant V_0 (zero-body), point V_1 (one-body), eight pairs (two-body), seven triplets (three-body) and seven quadruplets (four-body) cluster. We have checked that additional clusters (up to eight two-body, 15 three-body, 15 four-body, three five-body, and one six-body cluster) do not change results significantly. The magnitude of ECIs drops with increase of their spatial extend due to electronic screening in metals, as can be seen in Table II. We note for completeness that the largest pair cluster 8 and triangular cluster 7 (and the most compact four-body cluster 1) are not of crucial importance and could be removed without significant loss of accuracy of the SIM fit. Using this cluster expansion, we compute the hcp random solid-solution mixing energies, verify the hcp ground states, and construct the metastable hcp Ag-Al phase diagram.

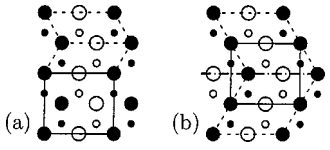

FIG. 5. (a) The unit cell of structure 6 (solid line), composed of two differently oriented unit cells of structure 3 (dashed line). (b) The domain boundary (dash-dotted line) of two orientations of structure 3.

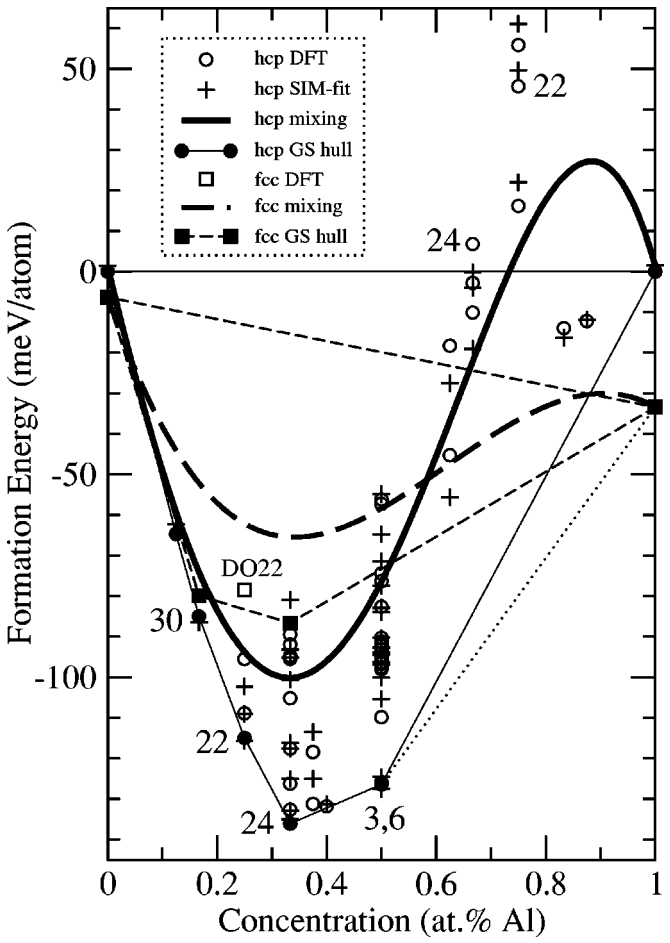

FIG. 6. Formation energies of the hcp structures listed in Table I (relative to the metastable hcp Ag and Al), DFT calculated (circles) and SIM fitted (crosses). Squares are the *ab initio* DFT energies of fcc structures. Filled symbols represent ground states (GS). The hcp and fcc SIM random solid solution mixing energies are plotted as the thick solid and large-dashed black lines, respectively.

C. Ag-Al ground states

The Ag-Al equilibrium ground states suggested from experiment are fcc-based Ag, complex cubic βMn-based Ag_3Al, hcp Ag_2Al, and fcc-based Al. The Al-rich Al-Ag alloy segregates into the fcc Al-rich terminal solid solution and the hcp intermediate γ phase (see Fig. 1). No phases other than hcp and fcc are known[1,2] in the composition range between Ag_2Al and Al. The fcc-based Ag-Al alloy was addressed in Ref. 11; the only fcc ground states found in this range are the equilibrium terminal fcc Al and metastable fcc Ag_2Al in $MoPt_2$ structure, which is 49 meV/atom higher in energy than the equilibrium hcp Ag_2Al ground-state structure 24.

The calculated fcc and hcp ground-state hulls are shown in Fig. 6 (filled symbols). Terminal Ag and Al solid phases are fcc based, while intermediate hcp Ag-Al ground states are lower in energy than the fcc-based ones. Structural parameters of lowest-energy hcp structures are given in Table III.

TABLE III. Structural parameters of the hcp Ag-Al lowest-energy structures. $\overline{a}$ is an average interatomic nearest neighbor distance (Å) within the hcp (0001) basal plane (or within the fcc (111) plane for the fcc Ag and Al, i.e., $\overline{a}=a_{lat}^{fcc}/\sqrt{2}$). c is the distance between adjacent hcp (0001) planes; $(c/\overline{a})_{ideal}=\sqrt{8/3}=1.633$. D_{xy} is the ratio of scales along vertical and horizontal directions in Fig. 4; except for structure 3, D_{xy} is the orthorombic distortion within the hcp basal plane. The orthorombic axes of structure 3 in Fig. 4 are rotated by $\pi/3$ and the orthorombic distortion is $\sqrt{(3-D_{xy}^2)/(3D_{xy}^2-1)}=0.937$. $\overline{v}$ is the calculated average volume per atom (Å^3).

Structure		$\overline{a}$(Å)	$c/\overline{a}$	D_{xy}	$\overline{v}$(Å^3)
fcc Ag		2.844			16.27
hcp Ag	1	2.838	1.644	1	16.29
Ag_5Al	30	2.824	1.638	1	15.98
Ag_3Al	22	2.834	1.635	1.016	15.87
Ag_2Al	24	2.827	1.608	0.970	15.74
Ag_3Al_2	"$n5$"	2.801	1.658	0.965	15.77
AgAl	3	2.790	1.682	1.033	15.80
AgAl	6	2.766	1.722	1.036	15.76
hcp Al	1	2.809	1.656	1	15.90
fcc Al		2.814			15.75

The average atomic volumes of hcp Ag-Al and elemental fcc Al given in Table III differ by less than 3%. The effects of atomic size mismatch and coherency stress in precipitated alloy were addresses in Ref. 7 and shown to be small. The static relaxations (both internal and external) are effectively incorporated in our SIM fit.

The hcp AgAl structures 3 and 6 have lower energy (see Fig. 6) than the phase segregated fcc Al—hcp Ag_2Al structure 24. Thus we predict an equilibrium ground state at composition 50 at. % Al not present in the assessed Ag-Al phase diagram[1,2] shown in Fig. 1.

We note that the AgAl structures 3 and 6 have an indistinguishable energy within our electronic-structure calculations. Interestingly, structure 6 can be viewed as a (periodically repeated) domain boundary within structure 3 (see Fig. 5) that costs no energy. Thus the AgAl ground state is degenerate due to zero-energy domain boundaries. In other words, there are innumberable AgAl ground-state configurations composed of domains of structure 3 oriented along the equivalent hcp (100), (010), and (110) directions within the basal plane.

We have calculated energies of all low-energy atomic configurations, as outlined in Sec. II C, and found no ground states of compositions $0.33<c_{Al}<1$ (i.e., between 33 and 100 at. % Al) other than Ag_2Al and AgAl. The hcp Ag_3Al_2 structure "$n5$" is near the tie line (within 1 meV), but does not become a ground state in our *ab initio* DFT calculations and SIM fit.

As can be seen in Fig. 4, hcp ground-state structures 30 (Ag_5Al) and 24 (Ag_2Al) have the same six-atom unit cells and differ only by Al↔Ag exchange at one site per cell. Ground-state structures 22 (Ag_3Al) and 6 (AgAl) have the same eight-atom unit cells with different stoichiometries. We then find that the hcp Ag-Al ground states have stoichiom-

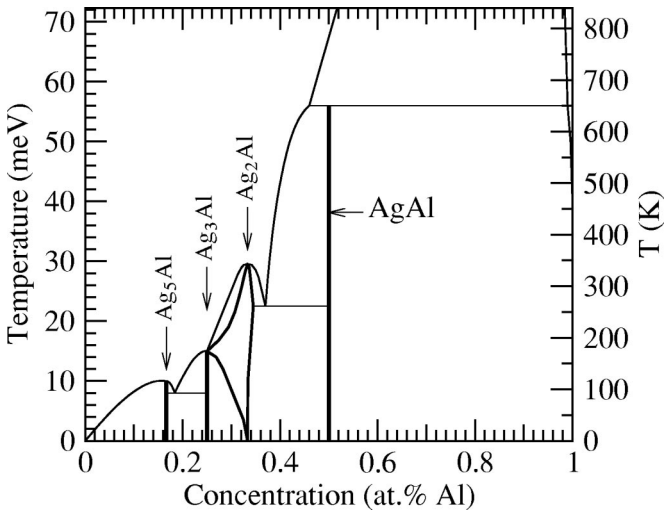

FIG. 7. First-principles calculated composition-temperature phase diagram for a metastable hcp Ag-Al alloy.

etries Ag_nAl, where $n=3k-1$ or $n=2^k-1$ (k is a positive integer), i.e., $n=1,2,3,5,7,\ldots$. As n increases, their energies approach the hcp solid-solution mixing energy. However, the hcp Ag_nAl ground states with $n\geqslant 7$ are irrelevant, because they all are higher in energy than the phase segregated fcc Ag–hcp Ag_5Al (structure 30). Taking into account complex cubic βMn-based Ag_3Al and fcc-based Ag and Al, we conclude that the only relevant equilibrium hcp ground states are Ag_2Al and AgAl.

D. Metastable hcp Ag-Al phase diagram

Given the ground states and effective Hamiltonian, we perform Monte Carlo simulations to construct the metastable hcp Ag-Al phase diagram. The calculated phase diagram (Fig. 7) shows the new ordered hcp AgAl phase at $c_{Al}=0.50$. The miscibility line above 650 K has a (maximum) critical point at $c_{Al}=0.86$ and $T=1640$ K, i.e., it extends far above the experimental melting temperature $T=1000$ K for disordered hcp γ phase and $T=840$ K (the top of our diagram in Fig. 7) for the phase segregated disordered hcp γ phase and fcc Al. We note that the computed boundary of the Ag-rich disordered hcp phase at $c_{Al}\approx 0.4$ and $T=473$ K approximately coincides with the corresponding boundary of the disordered hcp γ phase in the experimental assessed Ag-Al phase diagram in Fig. 1.[1,2]

The hcp AgAl phase at 50 at. % Al is stable below the peritectoid temperature $T=650$ K and has a very narrow compositional width (≈ 1 at. % at 260 K). This phase is pertinent to the equilibrium Ag-Al phase diagram.

The equilibrium ordered Ag_2Al phase is prolongated in composition from $c_{Al}=0.345$ at $T=260$ K to $c_{Al}=0.25$ at $T=174$ K; its (maximum) congruent point is at $c_{Al}=1/3$ and $T=350$ K. Long- and short-range orderings in Ag_2Al, as well as coherency stress and compositional effects within the hcp Ag_2Al precipitates, were addressed in Ref. 7, where agreement with the x-ray experiment[8] was demonstrated.

The ordered hcp Ag_3Al phase at $c_{Al}=1/4$ is (meta)stable below $T=174$ K. The ordered Ag_5Al phase at $c_{Al}=1/6$ is (meta)stable below $T=116$ K. Its fcc-based Ag_5Al analog is found[11,28] to influence the short-range order in the fcc α-phase Ag-rich solid solution of the same composition.

We note for completeness that there are other hcp ordered phases and ground states between hcp Ag and Ag_5Al of composition Ag_nAl ($n=7$, 11, 15, etc.), which, as we already noted in Sec. III C, are higher in energy than the phase segregated fcc Ag—hcp Ag_5Al; these Ag_nAl phases (omitted for clarity for $n\geqslant 7$) form a staircase under the boundary of (metastable) hcp Ag-rich terminal solid solution phase shown in Fig. 7. We also note that order-disorder transition temperatures in Fig. 7 are proportional to the energy differences between disordered solid-solution and ordered phases found in Fig. 6.

As we mentioned in Sec. III C, the equilibrium Ag-rich and Al-rich terminal solid solutions are fcc-based. Also, due to the existence of the intermediate equilibrium low-temperature Ag_3Al μ phase (extending from 21.2 to 24.3 at. % Al at 573 K and reported from experiment[29] to have complex cubic βMn structure, which may order below 623 K) and the high-temperature bcc Ag_3Al β phase, the hcp phase is not stable at compositions $c_{Al}<0.23$. Thus only the intermediate hcp ordered Ag_2Al and AgAl phases are relevant to the equilibrium Ag-Al phase diagram.

IV. DISCUSSION

The calculated formation energies of the ground states and solid solutions in Fig. 6 and the phase diagram in Fig. 7 are useful not only for prediction of equilibrium phases but also for understanding precipitation and for explaining experimental data. Below we compare the hcp and fcc solid-solution mixing energies, predict the composition range for disordered hcp precipitates, and explain the experimentally observed hcp precipitate composition range. Then we discuss structure and ordering tendencies relevant to precipitates and the new bulk AgAl phase.

A. Solid solution mixing energies and precipitate compositions

The hcp homogeneously random solid solution mixing energy curve (see Fig. 6) has a minimum around Ag_2Al, and is asymmetric in composition. This asymmetry is expected from the fact, that Al-rich structures 24 ($AgAl_2$) and 22 ($AgAl_3$) have energies above the phase segregated hcp Al-Ag, while the corresponding Ag-rich structures are the hcp ground states. Such an asymmetry makes the convergence of the cluster expansion slow, requiring a large number of structural energies and effective clusters.

The fcc-based homogeneously random solid solution mixing energies were reported in Ref. 11 and rescaled in Fig. 6 using the *ab initio* formation energies of fcc structures. The present calculations were full-potential, whereas the previous ones using the linear muffin-tin orbital method were more approximate.[11]

Both hcp- and fcc-based mixing energy curves are convex for Al-rich Al-Ag. This convexity indicates an incipient tendency for Al-rich alloys to form a miscibility gap and drive precipitation. Similar asymmetry and convexity of the ex-

perimentally measured at 1273 K formation enthalpy (heat) ΔH versus composition are observed in liquid Al-Ag alloys (see page 21 of Ref. 13).

The hcp and fcc mixing energies intersect at $c_{Al} \approx 0.58$; thus the formation of disordered hcp precipitates of compositions $c_{Al} < 0.58$ is energetically favorable. We note that the temperature of a homogeneously random (i.e., fully disordered) solid solution is formally infinite. At finite temperature short-range ordering results in lowering of mixing energies, which is more significant for the hcp phase; this further shifts compositions of just-formed hcp precipitates toward Al-rich compositions. The composition of well-equilibrated disordered hcp γ precipitates is determined by the tangent line drawn through the fcc Al and touching the hcp Al-Ag mixing energy curve at $c_{Al} \approx 0.4$; the same composition is given by the assessed Ag-Al equilibrium diagram[1,2] in Fig. 1.

The first-principles predicted composition range $0.40 < c_{Al} < 0.58$ for disordered hcp precipitates is in agreement with experiment.[6] In the experiment,[6] an Al-Ag alloy was annealed for 1 h at 823 K, immediately aged for 2–12 min at 673 K, cold-water quenched, and then annealed for 48 h at 433 K. The dispersive x-ray spectroscopy measurement showed an average composition of immediately formed precipitates approximately 58 at. % Al, significantly higher than 41 at. % Al given by the equilibrium Al-Ag phase diagram[1,2] in Fig. 1 or 33 at. % Al suggested in the previous experiment.[5]

B. AgAl phase and precipitate structure

The ground states in Fig. 6 and the phase diagram in Fig. 7 indicate that Al-rich Al-Ag alloys segregate into an ordered hcp AgAl phase and a terminal fcc Al phase at low temperatures ($T < 650$ K). However, the predicted equilibrium fully ordered hcp Ag_2Al and AgAl phases are not experimentally observed.

The Ag_2Al ground-state structure has been inferred from the measured SRO within the disordered hcp γ phase.[8] In Ref. 7, this Ag_2Al structure was verified as the ground state; short- and long-range ordering in Ag_2Al was calculated and compared to experiment; a remarkable quantitative agreement was found with the x-ray data[8,30] for bulk Ag_2Al. Also the coherency stress within the hcp precipitates was estimated.[7] As the atomic size in Table III is very similar in Ag, Al, and Ag-Al alloys, the coherency stress is small.

The predicted ordered hcp AgAl phase is difficult to observe experimentally. While the formation kinetics of a hcp precipitate is fast due to the large thermochemical driving force, the kinetics of forming long-range order within the precipitate is slow due to low temperatures and to the lack of vacancies that provide vacancy-assisted diffusion and ordering. An exact time scale for ordering kinetics depends crucially on saddle-point energies for vacancy-assisted diffusion. Because diffusion rate drops dramatically with decreasing temperature, as does the vacancy concentration, a long annealing time at low temperatures is needed for ordering. In addition, the unavoidable zero-energy domain boundary defects make the AgAl ground state degenerate and inhibit reaching a fully ordered state within a single precipitate. The ''ordered'' hcp AgAl phase should contain multiple domains, and therefore have no obvious LRO within the hcp basal planes.

Thus we propose an experiment on a Ag–50-at. % Al sample, rapidly quenched to provide excess vacancies needed for ordering and long-annealed below 650 K. Another possibility includes preparation of a sample in the predicted AgAl phase by a controlled-growth experiment, e.g. molecular beam epitaxy. High-resolution transmission electron microscopy should distinguish large ordered domains. We look forward to experimental verification of the predicted hcp AgAl phase.

V. CONCLUSION

We combined *ab initio* electronic-structure calculations with Monte Carlo simulation via SIM using the cluster expansion, and investigated the hcp Ag-Al ground states and constructed the metastable hcp Ag-Al phase diagram. We verified the previously reported equilibrium ordered hcp Ag_2Al phase[7] and found a new equilibrium hcp AgAl phase. The AgAl ground state is predicted to be degenerate due to zero-energy domain boundaries, and is expected to be relevant to precipitation.

We also compared hcp- and fcc-based solid-solution mixing energies and explained the experimentally observed composition range of the hcp γ precipitates.[6] The calculated mixing energies are found to be highly asymmetric versus composition, indicating an incipient tendency to precipitate. This is in agreement with the asymmetry of the experimentally measured enthalpy in the liquid phase.[13]

ACKNOWLEDGMENTS

We thank Mark Asta and Axel van de Waal for helpful communication. We acknowledge our support in part by ALCOA Foundation Grant, U.S. Department of Energy through the Frederick Seitz Materials Research Laboratory at the University of Illinois under Grant No. DEFG02-91ER45439, the National Science Foundation through Information Technology Research under Grant No. DMR-0121695 and through the UIUC Materials Computation Center (MCC) under Grant No. DMR-99-76550, and the IBM SURS equipment grant at the MCC.

*Electronic address: zarkevic@uiuc.edu

[1] A. McAlister, Bull. Alloy Phase Diagrams **8**, 526 (1987).

[2] *Desk Handbook: Phase Diagrams for Binary Alloys* edited by H. Okamoto (ASM International, Materials Park, OH, 2000).

[3] G. Petrenko, Zh. Russkogo Fiziko-Khimicheskogo Obshchestva (J. Rus. Phys.-Chem. Soc.) **46**, 176 (1914).

[4] G. Petrenko, Z. Anorg. Allg. Chem. **46**, 49 (1905).

[5] J.M. Howe, U. Dahmen, and R. Gronsky, Philos. Mag. A **56**, 31 (1987).

[6] K. Moore and J. Howe, Acta Mater. **48**, 4083 (2000).

[7] N.A. Zarkevich, D.D. Johnson, and A.V. Smirnov, Acta Mater. **50**, 2443 (2000).

[8] J. Neumann, Acta Metall. **14**, 505 (1966).
[9] Y. Kitano, K. Fujuwara, H. Kamiyahata, and Y. Komura, J. Phys. Soc. Jpn. **48** (1980).
[10] J.D. Mote, K. Tanaka, and J.E. Dorn, Trans. Metall. Soc. AIME **221**, 858 (1961).
[11] M. Asta and D.D. Johnson, Comput. Mater. Sci. **8**, 64 (1997).
[12] M. Asta and J. Hoyt, Acta Mater. **48**, 1089 (2000).
[13] R. R. Hultgren, P. D. Desai, D. T. Hawkins, M. Gleiser, and K. K. Kelley, *Selected Values of the Thermodynamic Properties of Binary Alloys* (American Society for Metals, Metals Park, Ohio, 1973).
[14] J.M. Sanchez, F. Ducastelle, and D. Gratias, Physica A **128**, 344 (1984).
[15] J. Connolly and A. Williams, Phys. Rev. B **27**, 5169 (1983).
[16] D. de Fontaine, Solid State Phys. **47**, 33 (1994).
[17] A. Zunger, in *Statics and Dynamics of Alloy Phase Transformations*, edited by P. Turchi and A. Gonis NATO Advanced Study Institute Series (Plenum, New York, 1994), p. 361.
[18] D. D. Johnson, in *Encyclopedia of Materials: Science & Technology*, edited by J. Dantzig (Pergamon Press, New York, 2002).
[19] G. Kresse and J. Hafner, Phys. Rev. B **47**, 558 (1993).
[20] G. Kresse, Ph.D. thesis, Technische Universität Wien, 1993.
[21] G. Kresse and J. Furthmüller, Comput. Mater. Sci. **6**, 15 (1996).
[22] G. Kresse and J. Furthmüller, Phys. Rev. B **54**, 11 169 (1996).
[23] D. Vanderbilt, Phys. Rev. B **41**, 7892 (1990).
[24] G. Kresse and J. Hafner, J. Phys.: Condens. Matter **6**, 8245 (1994).
[25] C. Wolverton, X.-Y. Yan, R. Vijayaraghavan, and V. Ozoliņš, Acta Mater. **50**, 2187 (2002).
[26] R. Vijayaraghavan, C. Wolverton, and L.Q. Chen, Phys. Rev. Lett. **88**, 125503 (2002).
[27] R. McCormack, M. Asta, D. de Fontaine, G. Garbulsky, and G. Ceder, Phys. Rev. B **48**, 6767 (1993).
[28] S-Y. Yu, B. Schönfeld, and G. Kostorz, Phys. Rev. B **56**, 8535 (1997).
[29] V.A. Yevsyukov, V.S. Postnikov, and I.M. Sharshakov, Fiz. Met. Metalloved. [Phys. Met. Metallogr.] **32**(2), 431 (1971).
[30] S-Y. Yu, B. Schönfeld, and G. Kostorz, in *Japan Institute of Metals Proceedings* (Sendai, Japan, 1999), Vol. 12 (JIMIC-3).